RSC Advances

ROYAL SOCIETY
OF CHEMISTRY

www.rsc.org/advances

Journal Name

ARTICLE

Chlorine-functionalized reduced graphene oxide for methylene blue removal†

Chubei Wang,*[a] Jianwei Zhou[a] and Liangliang Chu[a]

Chlorine-functionalized reduced graphene oxide was prepared by using graphene oxide and sulfuryl chloride as raw materials. It is firstly reported that hydroxyl group in graphene oxide can be substituted by chlorine in sulfuryl chloride. The product has wider pore size and average interlayer space, its surface area can be easily utilized. Adsorption data indicate that the material has high adsorption capacity on methylene blue. The adsorption process follows second-order rate and Bangham diffusion kinetic model. The adsorption of methylene blue preferably fitting the Langmuir adsorption isotherm suggests monolayer coverage of adsorbed molecules. The adsorption capacity of the product for methylene blue is 221.4 mg g^{-1} at room temperarure, which is significantly higher than those of reduced graphene oxide (80.0 mg g^{-1}) and active carbon (46.7 mg g^{-1}).

1.Introduction

Graphene composites have potential applications in the wastewater treatment system. The synergistic effects of graphene nanosheets and modifications improve the property.[1,2] There are many non-covalent modifications.[3,4] Pillared graphene was prepared by Külaots and Ye,[5,6] Külaots found that pillaring was a more effective method than crumpling for increasing surface area. However, non-covalent interactions (van der Waals, electrostatic or π–π stacking) are weak leading to unstable systems.

Graphene oxide (GO), derived from the oxidation of graphite, possesses abundant oxygenated functional groups, which offer reactive sites for covalent modification. The epoxide groups of GO undergo a nucleophilic substitution reaction with N-containing compunds to form composites.[7-11] The carboxyl groups can react with amine, secondary amine and other group.[12-18] The hydrogen of phenolic hydroxyl in GO can be substituted.[19-22] Hydroxyl group also can be initiated to grow polymer brushes form GO and reduced graphene oxide (RGO).[23-25] GO sheets also can be modified with siloxane coupling agent.[26-31] GO was functionalized with amino acids by the reaction between carboxylic groups, epoxides and the amine groups in amino acids.[32,33] The GO was treated with chloroacetic acid to convert the hydroxyl and epoxide groups to carboxyl groups.[34,35] Toluene-2,4-diisocyanate was applied to create anchor site on GO, which can lead to the derivatization of carboxyl and hydroxyl functional groups.[36] In all, the

chemical properties of these groups in GO are like those in organic compounds.

In this work, GO was treated by sulfuryl chloride (SO_2Cl_2) and then it was reduced by thermal reduction, the product was the chlorine-functionalized reduced graphene oxide (ClRGO). The OH groups in GO behave like those of phenol in substitution reactions. As well known, phenolic hydroxyl group can not react with sulfuryl chloride. To the best of our knowledge, there has been little report about that OH group in GO is substituted by chlorine in sulfuryl chloride.

2.Experimental

2.1 Materials

Pristine graphite was purchased from Qingdao BCSM Co., Ltd., (Qingdao, China), and sulfuryl chloride (SO_2Cl_2) was supplied by Shanghai Chemical Reagent Company (Shanghai, China). All other chemicals were of analytical grade and were purchased from Beijing Chemical Reagents Company (Beijing, China). All chemicals were used without further purification.

2.2 Synthesis of ClRGO and RGO

A mixture of GO (0.50 g) and acetonitrile (30 mL) was sonicated for 60 min. Water bath sonication was performed using a JL-60 DTH sonicator (100 W). Sulfuryl chloride (2.00 g, about 1.2 mL) was added to the GO solution at 75 °C under stirring for 2 h. The mixture was heated and refluxed for 5 h. The mixture was cooled down to ambient temperature, and then the mixture was poured in water (100 mL). The product was collected by filtration and washed several times with deionized water. The ClRGO was dried at 50 °C for 12 h to yield a black powder (0.31 g).

GO (0.20 g) was dispersed in water (500 mL) with the aid of ultrasonication, and then hydrazine hydrate (80 wt%, 20 mL)

[a] Institute of Energy and Fuel, Xinxiang University, Xinxiang, Henan 453003, China.Email: wangchubei@163.com, Fax: +86-373-3682028, Tel.: +86-373-3682028

was added at 100 °C for 24 h.[34–36] The product was collected by filtration and washed several times with deionized water. The RGO was dried at 50 °C for 10 h to yield a loose black powder (0.12 g).

2.3 Characterization

Scanning electron microscopy (SEM) and energy-dispersive X-ray (EDX) spectroscopy were performed using Hitachi S-4800 field emission and FEI-Quanta 200 scanning electron microscopes, respectively. High-resolution TEM (HRTEM) was performed on a JEOL JEM-2011 electron microscope operated at 200 kV, equipped with an Oxford Link ISIS energy dispersive X-ray spectroscopy (EDX) system, and a Gatan 794 camera. Fourier-transform infrared (FTIR) spectra were obtained on an FTS-40 (Bio-Rad, CA, USA). Raman spectra were recorded on a Renishaw InVia multi-channel confocal microspectrometer with 532 nm excitation laser. X-ray diffraction (XRD) measurements were obtained on an X'pert PRO diffractometer using Co Kα radiation. X-ray photoelectron spectroscopy (XPS) with monochromatized Al Kα X-ray (hν = 1486.6 eV) radiation (Thermo Fisher Scientific Co., ESCALAB 250, USA) was used to investigate the surface properties of the ClRGO. The shift in binding energies was corrected using the C 1s signal at 284.6 eV as the internal standard. Nitrogen sorption measurements were performed with ASAP 2020 V3.01H (Micromeritics, USA). Specific surface areas, pore volumes, and pore size distributions were calculated using the Brunauer–Emmett–Teller (BET) and density functional theory (DFT) models from the adsorption branches. Prior to measurement, the samples were outgassed under vacuum at 250 °C for ca. 10 h until the pressure was less than 5 μm Hg.

2.4 Adsorption

Batch adsorption experiments were performed using 500 mL glass bottles with a mixture of adsorbent (approximately 2 mg) and methylene blue (MB) solution (400 mL, 6 mg L^{-1} to 14 mg L^{-1}). The glass bottles were sealed with Teflon. The temperature of the solution was controlled to the desired value with a variation of ± 0.02 °C by adjusting the flow rate of thermostatically controlled water through an external glass-cooling spiral. The mixture was sampled in a series of intervals, and the concentration of the organic compound remaining in the mixture was measured after centrifugation. The concentration was measured by a UV/vis spectrometer. Values were calculated using the standard spectrophotometric method at the maximum absorbance of each compound.

3.Results and discussion

3.1 Structural features of the ClRGO

The morphologies and microstructures of ClRGO are characterized by SEM and TEM in Fig. **1**. The presence of wrinkles and folds on the sheet might be a characteristic feature of few-layered sheets in Fig 1a and 1b. The atomic-scale roughness might result from the chlorine-containing functional groups and residual oxygenated functional groups attached over ClRGO sheets. Thus, ClRGO is expected to be porous.

Some stacking pores are shown in Fig. 1c. The corresponding EDX spectrum revealed the presence of C, O and Cl, which imply that some OH groups in GO was substituted by chlorine. The atomic percentages of elements in ClRGO are in Table S1. Compared with phenolic compounds, GO has extended conjugation. Charge is easy to disperse in a conjugated system, and then the intermediate is more stable. GO can be reduced by thermal reduction at about 100 °C, this fact also confirms that the OH group in GO can leave. The OH group in GO might leave, and might be substituted by chlorine.

FTIR spectra further show substitution and reduction of GO to ClRGO in Fig. **2a**. ClRGO shows the skeletal vibration of unoxidized graphitic domains at 1580 cm^{-1}, alkoxy C–O at 1092 cm^{-1} and C–Cl at 653 cm^{-1}. The bond of carbon and chlorine forms in ClRGO. RGO shows the stretching vibrations of –OH groups at 3380 cm^{-1}, skeletal vibration of unoxidized graphitic domains at 1580cm^{-1}, and alkoxy C–O at 1120 cm^{-1}. The Raman spectra of ClRGO present a broadened G band at 1587 cm^{-1} in Fig. **2b**, because of the formation of a conjugated system. The G band at about 1580 cm^{-1} is associated with the vibration of sp^2 carbon atoms**.** The D band at about 1350 cm^{-1} related to the vibration of sp^3 carbon atoms of defects and disorder. The intensity of the D band at 1346 cm^{-1} of ClRGO increases substantially, indicating the decrease in size of the in-plane sp^2 domains, possibly due to the extensive substitution. There are more sp^3 carbon atoms in the ClRGO than these in RGO. When the hydroxyl group is substituted by chlorine and GO is reduced, the intensity of the D band increases further. The GO has more sp^3 carbon atoms than ClRGO, some sp^3 carbon atoms in ClRGO become sp^2 carbon atoms. This can also be due to defects introduced into the ClRGO during preparation.[40, 41] The I_D/I_G ratio of the ClRGO is approximately 1.34, which is higher than that of RGO (1.15). This result indicates that more graphene domains are formed on the ClRGO sheet when the oxygenated functional groups on sheet are removed.

The XRD patterns of RGO and ClRGO are shown in Fig. **3a**. ClRGO exhibits the intensity and broadness of the peak at 2θ = 24.8°, the average interlayer space of ClRGO is about 0.41 nm. The characteristic peak of RGO is at 27.6° (0.36 nm). Some OH group in graphene oxide is substituted by chlorine. The amount of OH group and hydrogen bond between sheets decrease, which weaken attractive force between sheets. Moreover, chlorine might also act as spacer and/or pillaring agent. The height of spacer or pillaring agent is about 0.33 nm (See ESI, Fig S1), which is about equal to the interlayer spacer of graphite. It might prevent graphene sheet close to each other, and then the interlayer space of ClRGO is widened.

The composites of the ClRGO were further analyzed by XPS. The core-level XPS signals of C 1s are shown in Fig. **3b**. The peak centered at approximately 284.6 eV originates from the graphitic sp^2 carbon atoms, whereas that located at 287.0 eV is caused by C–Cl and C–O. The peak of C=O in carboxylic acid is found at 288.8 eV. The peaks at the 200.4 and 201.9 eV are assigned to Cl 2 p$_{3/2}$ and Cl 2 p$_{1/2}$ in Fig. **3c**. The XPS survey spectra of the ClRGO show the presence of C, O and Cl elements in Fig. **3d**. The core-level XPS signals of C 1s are

similar to those of RGO, which also indicate that ClRGO is fully reduced.

The porosity of the ClRGO was also confirmed by nitrogen sorption. Nitrogen adsorption-desorption isotherm exhibits a characteristic IUPAC type IV curve in Fig. **4a**. The surface areas of ClRGO, RGO, and commercial activated carbon (AC) are 341.7, 319.9, and 420.4 m^2 g^{-1}, respectively, as obtained by fitting the isotherm to the BET model. Some pores and slits with small width in RGO type of materials are inaccessible to probe molecules used in surface area analysis (e.g. N$_2$, CO$_2$)[5]. RGO has little spacers and/or pillaring agents, some surface area can not be analyze, while ClRGO has spacers and/or pillaring agents, more surface area can be analyzed. The porosities of ClRGO, RGO, and AC can be further confirmed by porosity distribution analysis based on the original DFT in Fig. **4b**. The incremental pore volume of ClRGO is higher than those of RGO and AC within the ranges of 15 nm to 50 nm and 50 nm to 120 nm, respectively. The ClRGO might have relatively more macropores and mesopores. Moreover, the mesopores of the ClRGO have wider width than those of the RGO. RGO sheets are smooth and can close to each other. RGO can substantially form micropores but only a few mesopores (Fig. **4b**). ClRGO sheets with chlorine might be rough as shown in Fig **1**. Roughness, wrinkles, folds, and twists act as spacer and/or pillaring agent. Compared with RGO, ClRGO has more spacers and/or pillaring agents on ClRGO sheets, more mesopores with wide pore size and more macropores are formed between ClRGO sheets. The interlayer space of ClRGO is wider, which also improve the pore size. The stacked pore size of ClRGO is obviously improved, which might enhance adsorption capacity.

3.2 MB adsorption and adsorption mechanism

In the present investigation, pseudo-first-order, pseudo-second-order, intraparticle diffusion and Bangham diffusion kinetic models were tested to obtain the rate constants, equilibrium adsorption capacity, and adsorption mechanism.[42,43]

The adsorption curves of MB with ClRGO, RGO and AC are shown in Fig. **5a**. The removal of organic compound attains equilibrium after approximately 70 h. For the ClRGO, the adsorption capacity for MB is 221.4 mg g^{-1}, which is considerably larger than that of RGO (80.0 mg g^{-1}) and AC (46.7 mg g^{-1}). Although RGO and ClRGO have similar surface areas, ClRGO has a large adsorption capacity. This phenomenon may be due to the fact that pore blockage may occur for adsorbents with small pore diameters because of the aggregation of bulky molecules in the pore orifice.[44,45] Therefore, the full surface area of RGO cannot be utilized, reducing the effectiveness of adsorption. ClRGO has more mesopores and macropores, and wider pore size than RGO. The results show that a large surface area is not vital for high adsorption capacities as is commonly believed; instead, large pore sizes are principally important for effective dye uptake, which is consistent with previous reports.[19, 21]

The fitting results obtained from different models are summarized in Table **1**. The correlation coefficients for the pseudo-first-order models are 0.985, 0.974, 0.989, 0.966, and 0.986. Significant differences exist between the calculated q_{cal}

values and experimental q_{exp} values. For the MB with high correlation coefficients of R^2 = 0.995, 0.996, 0.993, 0.993, 0.997 (fitting curve is shown in Fig. **5b**), the pseudo-second-order model provides good correlation for the adsorption of organic compounds on ClRGO. For the pseudo-second-order model, the calculated q_{cal} values agree well with the experimental q_{exp} values.

The intraparticle diffusion models have low correlation (0.952, 0.956, 0.974, 0.972, and 0.949), indicating that these models are not suitable for describing the MB adsorption on ClRGO. k_{dif} increases but C decreases with temperature. These results indicate that the rate of MB removal increases with increasing temperature. None of the plots passes through the origin, indicating that the intraparticle diffusion is part of the adsorption but is not the only rate-controlling step.

Since the uptake of MB on ClRGO slowed down during the later stages of the adsorption, Bangham diffusion model was tested for its applicability for MB adsorption on ClRGO. The parameters α and k$_0$ were calculated from the slope and intercept for five different temperatures and are displayed along with the R^2 values (Fig. **5c**, and Table **1**). The plots reveal that the lines at 298 K are not straight for ClRGO indicating that pore diffusion is not solely rate-determining in Fig. **5c**. The diffusion speed of MB in solution might also affect adsorption. At high temperatures, such as 308, 318, 328, and 338 K, the R^2 values (0.991, 0.997, 0.996, and 0.991) are high. The diffusion speed of MB in solution is high, pore diffusion mainly affect adsorption. Bangham diffusion kinetic model was found applicable to this adsorption system in terms of relatively high regression values.

The Langmuir, Freundlich, and Dubinin-Radushkevich (D-R) isotherm models are applied to simulate and understand the adsorption mechanism of MB at different temperatures,[42] the fitting results from different models are summarized in Table **2**. The Langmuir model parameters and the statistical fits of the adsorption data are shown in Fig. **5d**. The high regression coefficient confirms that the Langmuir isotherm best represents the equilibrium adsorption of MB to ClRGO at different temperatures. The excellent fit of the Langmuir isotherm to the experimental data at all temperatures confirms that the adsorption is monolayer. The adsorption of each molecule has equal activation energy, and the sorbate-sorbate interaction is negligible. The constant R_L lies within the favorable limit (between 0 and 1), indicating a favorable process. In addition, q_m increases with temperature. The Langmuir constant (b) also increases with temperature. Overall, the information obtained specifies an endothermic nature of the existing process. The monolayer adsorption capacity of graphene for MB as obtained from the Langmuir isotherm at 338 K is 357.1 mg g^{-1}, and the experimental q_{exp} value is 355.6 mg g^{-1}.

K_F and n are the Freundlich parameters related to adsorption capacity and adsorption intensity, respectively. The value of $1/n$ is lower than 1, indicating a normal Langmuir isotherm.

The D-R model is related to the porous structure of the sorbent and apparent energy of adsorption, the model is also used to distinguish between physical and chemical adsorption of MB.[42] The magnitude of E is lower than 8.0 kJ mol^{-1} at all tested

temperatures, indicating that the adsorption mechanism is physical adsorption.

4.Conclusions

Hydroxyl group in graphene oxide can be substituted by chlorine in sulfuryl chloride. ClRGO will be an important intermediate for preparing Grignard reagents and other compounds. ClRGO has wider pore size and average interlayer space than RGO, and it enhances capability for MB. Adsorption data indicate that the material has high adsorption capacity on methylene blue. The adsorption process follows second-order rate and Bangham diffusion kinetic model. The adsorption of MB preferably fitting the Langmuir adsorption isotherm suggests monolayer coverage of adsorbed molecules.

Acknowledgements

References

1   C. Chao, J. D. Liu, J. T. Wang, Y. W. Zhang, B. Zhang, Y. T. Zhang, X. Xiang and R. F. Chen, *ACS Appl. Mater. Inter*., 2013, **5**, 10559.
2   C. Chao, B. Zhang, R. Zhai, X. Xiang, J. D. Liu and R. F. Chen, *ACS Sustain. Chem. Eng*., 2014, **2**, 396.
3   C. X. Gui, Q. Q. Wang, S. M. Hao, J. Qu, P. P. Huang, C. Y. Cao, W. G. Song and Z. Z. Yu, *ACS Appl. Mater. Inter*., 2014, **6**, 14653.
4   C. Zhang, R. Z. Zhang, Y. Q. Ma, W. B. Guan, X. L. Wu, X. Liu, H. Li, Y. L. Du and C. P. Pan, *ACS Sustain. Chem. Eng*., 2015, **3**, 396.
5   F. Guo, M. Creighton, Y.T. Chen, R. Hurt and I. Külaots, *Carbon*, 2014, **66**, 476.
6   Z.M. Wu, L. Zhang, Q.Q. Guan, P. Ning and D.Q. Ye, *Chem. Eng. J*., 2014, **258**, 77.
7   G. G. Liu, S. Gui, H. Zhou, F. T. Zeng, Y. H. Zhou and H. Q. Ye, *Dalton Trans*., 2014, **43**, 6977.
8   Y. S. Fu, J. W. Zhu, C. Hu, X. D. Wu and X. Wang, N*anoscale*, 2014, **6**, 12555.
9   M. M. Sk and C. Y. Yue, *RSC Adv*., 2014, **4**, 19908.
10 G. Erdenedelger, T. Lee, T. D. Dao, J. S. Kim, B. S. Kim and H. M. Jeong, *J. Mater. Chem. A*, 2014, **2**, 12526.
11 F. Zhang, B. Wang, S. F. He and R. L. Man, *J. Chem. Eng. Data*, 2014, **59**, 1719.
12 M. Jana, P. Khanra, N. C. Murmu, P. Samanta, J. H. Lee and T. Kuila, *Phys. Chem. Chem. Phys*., 2014, **16**, 7618.
13 R. Rajesh, S. S. Kumar and R. Venkatesan, *New J. Chem*., 2014, **38**, 1551.
14 R. K. Yadav, J. O. Baeg, A. Kumar, K. Kong, G. H. Oh and N. J. Park, *J. Mater. Chem. A*, 2014, **2**, 5068.
15 W. Ai, X. H. Cao, Z. P. Sun, J. Jiang, Z. Z. Du, L. H. Xie, Y. L. Wang, X. J. Wang, H. Zhang, W. Huang and T. Yu, *J. Mater. Chem. A*, 2014, **2**, 12924.
16 H. Y. Qin, T. Gong, Y. J. Cho, C. G. Lee and T. Kim, *Polym. Chem.*, 2014, **5**, 4466.
17 J. Yang, J. X. Wu, Q. F. Lü and T. T. Lin, *ACS Sustain. Chem. Eng*., 2014, **2**, 1203.
18 T. Wu, X. Y. Xu, L. Zhang, H. B. Chen, J. P. Gao and Y. Liu, *RSC Adv***.**, 2014, **4**, 7673.
19 C. B. Wang, J. Ni, J. W. Zhou, J. L. Wen and X. B. Lü, *RSC Adv*., 2013, **3**, 23139.
20 C. B. Wang, J. W. Zhou, J. Ni , Y. L. Cheng, and H. Li, *Chem. Eng. J*., 2014, **253**, 130.
21 C. B. Wang, J. Ni and J. W. Zhou, *Mater. Technol*., 2014, **29**, 252.
22 B. T. McGrail, B. J. Rodier and E. Pentzer, *Chem. Mater.*, 2014, **26**, 5806.
23 J. Chen, P. Xiao, J. C. Gu, Y. J. Huang, J. W. Zhang, W. Q. Wang and T. Chen, *RSC Adv*., 2014, **4**, 44480.
24 X. B. Zhao and P. Liu, *Langmuir*, 2014, **30**, 13699.
25 Z. Z. Liu, S. J. Zhu, Y. J. Li, Y. S. Li, P. Shi, Z. Huang and X. Y. Huang, *Poly. Chem*., 2015, **6**, 311.
26 C. J. Madadrang, H. Y. Kim, G. H. Gao, N. Wang, J. Zhu, H. Feng, M. Gorring, M. L. Kasner and S. F. Hou, *ACS Appl. Mater. Inter*., 2012, **4**, 1186.
27 M. Z. Iqbal, M. S. Katsiotis, S. M. Alhassan, M. W. Liberatore and A. A. Abdala, *RSC Adv*., 2014, **4**, 6830.
28 H. L. Su, Z. F. Li, Q. S. Huo, J. Q. Guan and Q. B. Kan, *RSC Adv*., 2014, **4**, 9990.
29 M. A. Nasseri, A. Allahresani and H. Raissi, *RSC Adv*., 2014, **4**, 26087.
30 S. Verma, M. Aila, S. Kaul and S. L. Jain, *RSC Adv*., 2014, **4**, 30598.
31 H. M. Liu, Y. Guo, X. S. Wang, Y. K. Li, X. J. Liang and X. Liu, *Anal. Methods*, 2015, **7**, 135.
32 H. J. Zhu, Y. J. Zhang, L. L. Zhang, T. Yu, K. Zhang, H. Jiang, L. J. Wu and S. H. Wang, *J. Mater. Chem. C*, 2014, **2**, 7126.
33 W. J. Liu, Y. K. Wang and Z. H. Li, *Chem. Commun*., 2014, **50**, 10311.
34 P. Kumar, B. Sain and S. L. Jain, *J. Mater. Chem. A*, 2014, **2**, 11246.
35 P. Kumar, G. Singh, D. Tripathi and S. L. Jain, *RSC Adv*., 2014, **4**, 50331.
36 A. Gupta, G. Chen, P. Joshi, S. Tadigadapa and P. C. Eklund, *Nano Lett*., 2006, **6**, 2667.
37 C. Gomez-Navarro, R.T. Weitz, A. M. Bittner, M. Scolari, A. Mews, M. Burghard, K. Kern, *Nano Lett*., 2007, **7**, 3499.
38 H. A. Becerril, J. Man, Z. Liu, R. M. Stoltenberg, Z. Bao, Y. Chen, *ACS Nano*, 2008, **2**, 463.
39 G. Eda, G. Fanchini, M.Chhowalla, *Nature Nanotechnol*., 2008, **3**, 270.
40 F. B. Meng, H. Ishida and X. B. Liu, *RSC Adv*., 2014, **4**, 9471.
41 Z. H. Ni, H. M. Wang, Y. Ma, J. Kasim, Y. H. Wu and Z. X. Shen, *ACS Nano*, 2008, **2**, 1033.
42 S. Vasudevan and J. Lakshmi, *RSC Adv*., 2012, **2**, 5234.
43 C. Aharoni, S. Sideman and E. Hoffer, *J. Chem. Technol. Biotechnol*., 1979, **29**, 404.
44 M. Valix, W. H. Cheng and G. McKay, *Langmuir*, 2006, **22**, 4574.
45 H. L. Parker, A. J. Hunt, V. L. Budarin, P. S. Shuttleworth, K. L. Miller and J. H. Clark, *RSC Adv*., 2012, **2**, 8992.

Graphical Abstract
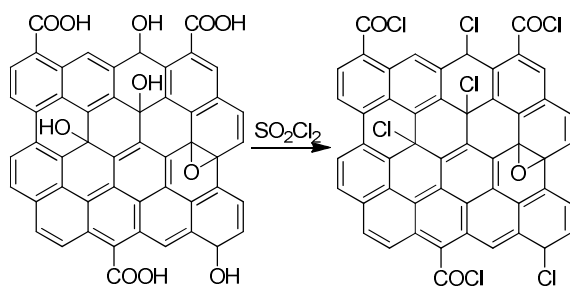
Hydroxyl group in graphene oxide can be substituted by chlorine in sulfuryl chloride at mild condition.
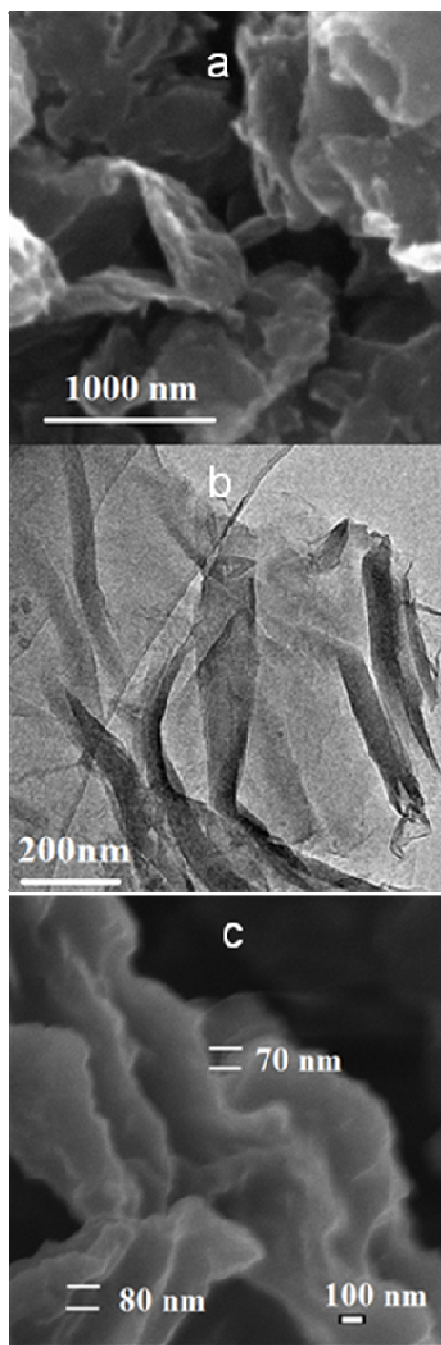
Fig. 1 Images of ClRGO. Image (SEM) (a) and. Images (TEM) of ClRGO (b, c)

RSC Advances Accepted Manuscript
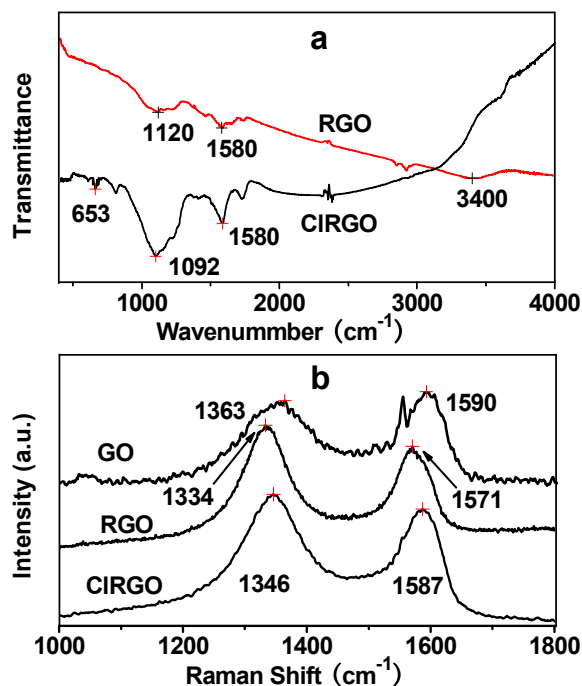
Fig. 2 FTIR spectra of RGO and ClRGO (a), Raman spectra of GO, RGO and ClRGO (b)
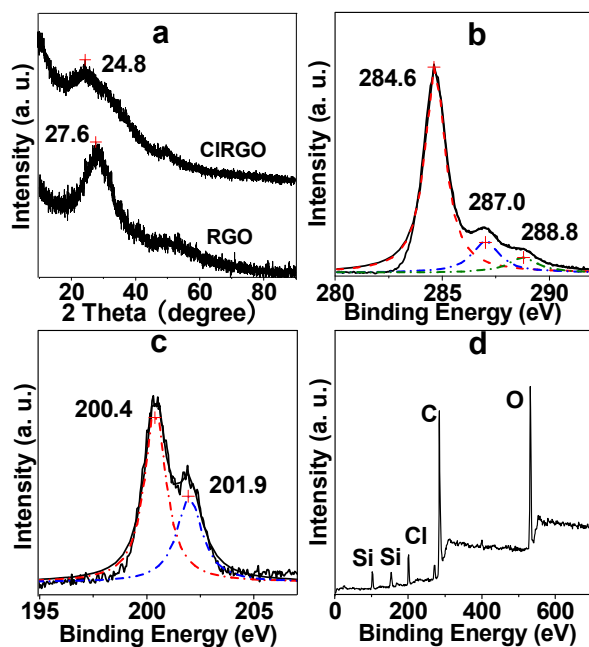
Fig. 3 XRD patterns of ClRGO and RGO (a), Core-level XPS spectra of C 1s (b) and Cl 2 p (c) of ClRGO, XPS survey spectra (d) of ClRGO
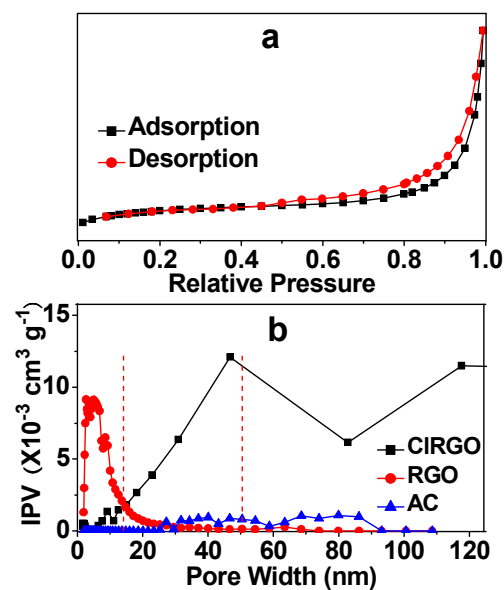
Fig. 4 Typical nitrogen adsorption and desorption of ClRGO (a) and pore size distribution curves of ClRGO, RGO, and AC (b). IPV = Incremental Pore Volume

Journal Name

ARTICLE
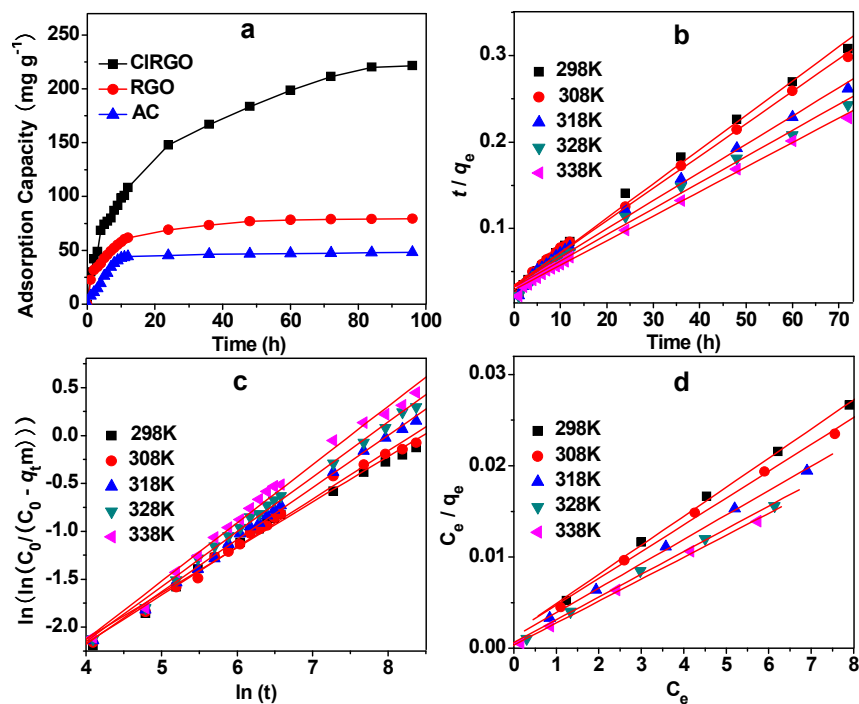
Fig. 5 Adsorption of MB by ClRGO, RGO, and AC (a). Conditions: concentration = 8 mg L^{-1} and room temperature. Adsorption kinetics of MB by ClRGO for pseudo-second order (b). Conditions: concentration = 8 mg L^{-1}. Bangham's diffusion plots for the removal of MB at different temperature (c). concentration = 8 mg L^{-1}. Langmuir plot (C_e / q_e vs. C_e) for MB adsorption by ClRGO at different temperatures (d). Concentration: concentration = 6 mg L^{-1} to 14 mg L^{-1}

Table 1 Parameters obtained from different kinetic models of MB[a]

Models and equations	Temperature	Parameters			R^2
		K_1 ($\times 10^{-2}$ min^{-1})	q_{cal} (mg g^{-1})	q_{exp} (mg g^{-1})	
pseudo-first-order	298K	3.29	178.1	248.9	0.985
$\ln (q_e - q_t) = \ln (q_e) - k_1 t$	308K	2.96	195.0	268.7	0.974
	318K	2.94	234.1	305.9	0.989
	328K	2.73	267.6	332.7	0.966
	338K	2.82	256.3	355.6	0.986
		K_2 ($\times 10^{-4}$ g mg^{-1} min^{-1})	q_{cal} (mg g^{-1})	q_{exp} (mg g^{-1})	
pseudo-second-order	298K	4.91	250.0	248.9	0.995
$t/q_t = 1/k_2 q_e^2 + t/q_e$	308K	4.04	270.3	268.7	0.996
	318K	3.18	303.0	305.9	0.993
	328K	2.80	333.3	332.7	0.993
	338K	2.71	357.1	355.6	0.997
		k_{dif} (mg g^{-1} min$^{-1/2}$)		C (mg g^{-1})	
Intraparticle diffusion	298K	24.59		42.3	0.952
$q_t = k_{dif} t^{1/2} + C$	308K	26.78		36.7	0.956
	318K	31.02		31.0	0.974
	328K	33.54		33.8	0.972
	338K	36.14		37.6	0.949
		k_0		α	
Bangham diffusion	298K	0.0894		0.476	0.985
$\ln (\ln (C_0/(C_0 - mq_t)))$	308K	0.0767		0.502	0.991
$= \ln (k_0 m/V) + \alpha \ln (t)$	318K	0.0637		0.546	0.997
	328K	0.0588		0.573	0.996
	338K	0.0521		0.609	0.991

[a] concentration = 8 mg L^{-1}

Table 2 Constant parameters and correlation coefficients calculated for different adsorption isotherm models at different temperatures for MB adsorption

Models and equations	constants		298K	308K	318K	328K	338K
	q_m (mg g^{-1})		312.5	344.8	370.4	400.1	416.7
Langmuir	b (L mg^{-1})		1.61	1.88	2.25	4.17	6.00
$C_e /q_e = 1/q_m b + C_e /q_m$	R_L	$C_0 = 6$mg/L	0.094	0.081	0.069	0.038	0.027
$R_L = 1/(1 + bC_o)$		$C_0 = 8$mg/L	0.072	0.062	0.053	0.029	0.020
		$C_0 = 10$mg/L	0.058	0.051	0.043	0.023	0.016
		$C_0 = 12$mg/L	0.049	0.042	0.036	0.020	0.014
		$C_0 = 14$mg/L	0.042	0.037	0.031	0.017	0.012
	R^2		0.998	0.996	0.998	0.997	0.998
Freundlich	K_F (mg g^{-1} (L mg^{-1})$^{1/n}$)		229.5	250.9	285.4	321.4	350.5
$\ln (q_e) = \ln (K_F) + (1/n)\ln (C_e)$	n^{-1}		0.121	0.109	0.105	0.102	0.092
	R^2		0.981	0.921	0.984	0.987	0.977
Dubinin-Radushkevich	q_s (mol g^{-1})		0.90	0.95	1.07	1.16	1.22
$\ln (q_e) = \ln (q_s) - B\varepsilon^2$	B ($\times 10^{-2}$ mol^2 KJ^{-2})		9.2	8.5	6.97	1.66	0.98
$\varepsilon = RT\ln (1+1/C_e)$	E (KJ mol^{-1})		2.3	2.4	2.7	5.5	7.1
$E = (2B)^{-1/2}$	R^2		0.794	0.789	0.923	0.830	0.919